

Dalton Transactions

Accepted Manuscript



This is an *Accepted Manuscript*, which has been through the Royal Society of Chemistry peer review process and has been accepted for publication.

Accepted Manuscripts are published online shortly after acceptance, before technical editing, formatting and proof reading. Using this free service, authors can make their results available to the community, in citable form, before we publish the edited article. We will replace this *Accepted Manuscript* with the edited and formatted *Advance Article* as soon as it is available.

You can find more information about *Accepted Manuscripts* in the [Information for Authors](#).

Please note that technical editing may introduce minor changes to the text and/or graphics, which may alter content. The journal's standard [Terms & Conditions](#) and the [Ethical guidelines](#) still apply. In no event shall the Royal Society of Chemistry be held responsible for any errors or omissions in this *Accepted Manuscript* or any consequences arising from the use of any information it contains.

Synthesis and aggregation behaviour of luminescent mesomorphic zinc(II) complexes with 'salen' type asymmetric Schiff base ligand

Sutapa Chakraborty,^a Chira R. Bhattacharjee,^{*a} Paritosh Mondal,^a S. Krishna Prasad,^b and D. S. Shankar Rao^b

^a *Department of Chemistry, Assam University, Silchar 788011, Assam, India.*

^b *Centre for Nano and Soft Matter Sciences, Jalahalli, Bangalore 560013, India.*

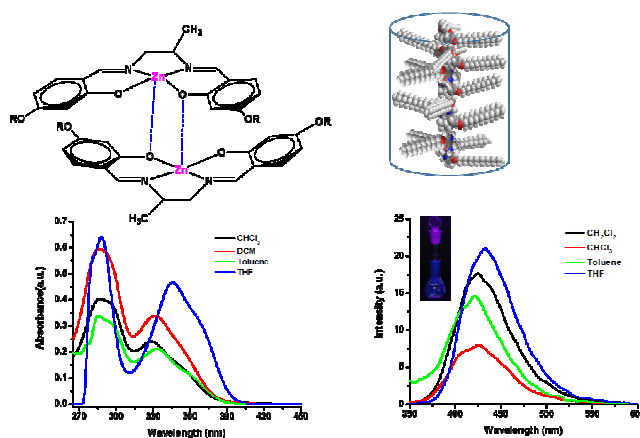
** Corresponding author. Tel.: +91-03842-270848; fax: +91-03842-270342*

Email: crbhattarjee@rediffmail.com

Table of Contents

Synthesis and aggregation behaviour of luminescent mesomorphic zinc(II) complexes with ‘salen’ type asymmetric Schiff base ligand

Sutapa Chakraborty,^a Chira R. Bhattacharjee,*^a Paritosh Mondal,^a S. Krishna Prasad,^b and D. S. Shankar Rao^b



Mesomorphism and solvent dependent aggregation behaviour of a new series of photoluminescent Zn(II)-salen type asymmetric Schiff base complexes have been investigated.

Abstract

A new series of photoluminescent Zn(II)-salen type asymmetric Schiff base complexes, [ZnL], $H_2L=[N,N'$ -bis-(4-n-alkoxysalicylidene)- 1,2-diaminopropane] (n = 12, 14 and 16) have been accessed and their mesomorphic and photophysical properties investigated. Though the ligands are non-mesomorphic, coordination to Zn^{2+} ion induces liquid crystalline behaviour. The complexes exhibited a lamello-columnar phase (Col_l) as characterized by variable temperature powder X-ray diffraction (XRD) study. Intense blue emissions were observed for the complexes at room temperature in solution, solid and in the mesophase. Aggregation properties of the complexes were explored in different solvents through absorption and photoluminescence studies. While de-aggregation to monomers occurred in coordinating solvents due to axial coordination to Zn(II), aggregates were formed in the solution of non-coordinating solvents. Density functional theory (DFT) computation carried out on a representative complex using GAUSSIAN 09 program at B3LYP level suggested a distorted square planar geometry. The results of time-dependent DFT (TD-DFT) spectral correlative study showed the electronic properties of the complex molecule to be in compliance with the spectral data.

Keywords: Metallomesogen; Zn(II); photoluminescence; aggregation; density functional theory.

1. Introduction

Transition metal-salen complexes have been a recurrent theme in synthetic co-ordination chemistry, yet interest in this field continue unabated possibly due to their wide applicability being unfolded in recent times.¹⁻⁴ A plethora of salen based complexes are now known to act as efficient catalysts both in homogeneous and heterogeneous reactions for asymmetric ring-opening of epoxides, aziridination, cyclopropanation, oxidation, reduction reaction of ketones, epoxidation of olefins, formation of cyclic and linear polycarbonates, catalytic enantio-selective and diastereoselective redox reactions and Diels–Alder reactions.⁵⁻⁸ Metal salen complexes are also efficient entities to study interactions with DNA leading to the development of sensitive chemical probes for DNA.⁹⁻¹² Besides, such systems are also known to exhibit interesting fluorescence,¹³⁻¹⁷ magnetic,^{17,18} non-linear optical¹⁹⁻²¹ and liquid crystalline properties²²⁻³⁰ and act as electrochemical sensors.³¹⁻³³ Metallomesogens based on Zn(II)-salen complexes are quite intriguing because of the possibility of combining luminescence with liquid crystallinity to generate newer systems with exotic multifunctional properties.³⁴⁻³⁷ Spacer group modification can lead to substantial change in mesophase as well as photophysical behavior in such hemi-disc shaped complexes.³⁴⁻³⁷ In past few years we have reported some novel fluorescent liquid crystalline Zn(II)-salen complexes with different spacer groups showing hexagonal, rectangular and rectangular/oblique columnar mesomorphism.³⁵⁻³⁷ Creating a minor modification at the central aromatic ring (spacer), new symmetry as well as newer organization in the mesophase could be achieved.³⁵⁻³⁷

Zn(II)-salen complexes and their derivatives also facilitate various structures which may be utilized for sensory materials for detection of alkaloids³⁸ and nitro aromatics,^{39,40} recognition of biologically relevant anions,⁴¹ selective receptors for tertiary amines,⁴² self-assembled heteromultimetallics,^{43,44} supramolecular box-shaped assemblies,^{45,46} molecular templates in catalytic studies,^{47,48} dopants for high performance OLEDs⁴⁹⁻⁵¹ and the exploration of their unique second-order nonlinear optical properties.^{19,20} High Lewis

acidity of the co-ordinatively unsaturated Zn^{2+} ion is believed to be the key to such behavior. Pentacoordinate nature of the Zn^{2+} ion boosted by the rigid geometry of the salen framework facilitates axial binding of donor ligands resulting in substantial variations in the optical absorption behaviour and enhanced fluorescence emission. In the absence of axial ligand, coordinative saturation is achieved through intermolecular $Zn\cdots O$ interactions involving the phenolate oxygen atoms of the salen ligand acquiring a square based pyramidal structure.^{52,55}

In continuation of our pursuit in designing photoluminescent metallomesogens, we report herein a new series of Zn(II) complexes of asymmetric 'salen' based N,N'-bis-(4-n-alkoxysalicylidene)-1,2-diaminopropane ligands. Induction of mesomorphism and photoluminescence via coordination to Zn(II) ion has been demonstrated. All the complexes are blue light emitters both in the solid state as well as in solution. The complexes all exhibited aggregate formation in non-coordinating solvents while only monomer is favoured in coordinating solvents. Density functional theory (DFT) calculations carried out using GAUSSIAN 09 program at B3LYP level revealed a distorted square planar geometry around the metal center in the complexes. Time-dependent DFT spectral correlative study was undertaken to account for the electronic transitions in the complexes.

2. Results and Discussion

2.1. Synthesis and structural assessment

Condensation of 4-alkoxy substituted aldehyde with the unsymmetrical amine, 1,2-diamino propane afforded the 'salen' type asymmetric Schiff base ligands. The strategy implemented for the synthesis of Schiff base ligands, [N,N'-bis-(4-n-alkoxysalicylidene)- 1,2-diaminopropane], hereafter abbreviated as ndap (n = 12, 14 and 16 is the number of carbon atoms in alkyl chains; dap = 1,2-diaminopropane) and the mononuclear complexes (Zn-ndap) is summarized in Scheme-1. The structure of the ligands and the corresponding Zn(II) complexes were probed by elemental analyses, UV-visible, FT-IR and ¹H NMR

spectroscopy. A broad band at $\sim 3370\text{cm}^{-1}$ attributed to the phenolic -OH group, is observed in the FT-IR spectra of the ligands (ndap). The C=N stretching vibration of the ligands are located in the region of $1653\text{-}1655\text{cm}^{-1}$. Upon complexation, the shift of $\nu_{\text{C=N}}$ mode to lower wave number, $\sim 1638\text{cm}^{-1}$ ($\Delta\nu \approx 16\text{cm}^{-1}$) and absence of $\nu_{\text{O-H}}$ mode attest to the deprotonation of the Schiff-base prior to coordination of azomethine nitrogen and phenolate oxygen to the Zn^{2+} ion. The ^1H NMR spectra of the ligands showed two characteristic signals, at $\delta = 11.45\text{ppm}$, corresponding to the OH proton, and at ~ 8.22 and 8.18ppm due to the resonance of two asymmetric imine protons. The ^1H NMR spectra of the corresponding Zn(II) complexes did not exhibit any signal for the phenolic -OH proton. Additionally, an up field shift ($\sim 0.56\text{ppm}$) in the peak position of the -N=CH protons further validated azomethine nitrogen coordination.

2.2. Mesomorphic study

The mesophase behaviour of the compounds has been investigated by polarizing optical microscopy (POM), differential scanning calorimetry (DSC) and variable temperature powder XRD techniques. Free ligands (ndap) are non-mesomorphic presumably owing to greater conformational flexibility. However, upon complexation with Zn(II) metal ion, mesomorphism is induced due to enhanced rigidity of the Schiff base ligand framework. The phase sequence, transition temperatures and associated enthalpies for the Zn(II) complexes are presented in Table 1. The complexes all exhibited enantiotropic liquid crystalline behavior. On cooling from the isotropic melt, a grainy texture was observed at 125°C (Figure 1). The DSC thermogram of the complexes Zn-14dap and Zn-16dap (Figure 2) exhibited two transitions each in the heating and cooling cycle. In the cooling scan, the grainy texture at the mesophase remains unaltered till ambient temperature slowly freezing into a glassy state. For the Zn-12dap complex, two additional peaks observed in the heating cycle were ascribed to crystal-crystal transitions. No isotropic liquid-mesophase transition could be detected in the cooling cycle (Table 1). This might be due to the partial vitrification of the mesophase. Viscous natures of the complexes tend to affect the molecular

mobility causing a pronounced hysteresis in the phase transition temperature in all the cases. A gradual decrease in the clearing temperature was observed with increasing number of carbon atoms in the pendant alkoxy arm. The isotropic liquid to mesophase transition temperature also displayed similar trends with increasing chain length. Repeated heating and cooling scans confirmed the reversibility of the thermal behaviour.

Variable temperature powder XRD study of a representative complex, Zn-16dap was carried out both in the mesophase and at room temperature. The X-ray diffraction pattern recorded at 100°C (Figure 3a, Table 2) contained several sharp and intense Bragg reflections in the small-angle region and two broad scattering halos (visualized by profile fitting of the data) in the wide-angle region. The broad maxima centered around 4.7 Å and 4.0 Å correspond, respectively, to the lateral short-range order of the molten chains and the molecular cores confirming the liquid nature of the mesophase. The sharpness of the small-angle reflections indicates long-range correlation of the structure. However, these reflections do not conform to either a purely lamellar or purely columnar structure. The first three reflections (at 34.1, 17.1 and 11.4 Å) being in the reciprocal spacing ratio 1:2:3, point to a well-defined layered structure. In contrast the remaining two sharp reflections observed at 9.8 Å and 8.5 Å cannot be ascribed to a lamellar form, but can be explained by invoking a columnar ordering. Since these peaks are much less intense than the primary layer peak, they can be considered to be arising due to 2-D columnar modulation of the layers. A mesophase exhibiting structural features which is a combination of the lamellar and columnar features has been referred to as a lamello-columnar (Col_l) phase.^{24,26-28,30} Symmetric 4-alkoxy substituted Schiff base containing ethylene diamine spacer complexed to Pt²⁺, Cu²⁺, VO²⁺ and Ni²⁺ have also been shown to exhibit Col_l phases though the 1D ordering is more pronounced in these cases.^{24,27,28,30} Though the corresponding Zn(II) complexes have been documented, the mesomorphic properties are not reported.⁵² The low intensity for second wide-angle halo expected due to interaction between the rigid part of one mesomorphic unit and its next nearest neighbour, suggests weaker correlation between the

cores within the column in the mesophase. Enhanced flexibility associated with aliphatic spacer group bearing the 'methyl' substituent is believed to induce bending and twisting deformations, with the resulting fluctuations reducing the core-core correlations.^{56,57} Similar behaviour has also been noticed for previously reported analogous Zn(II) and Cu(II) complexes with asymmetric methyl substituted aromatic spacer.^{22,37}

Spacer group substitution can have marked influence on the mesomorphic properties in the 'salen type' zinc(II) complexes. In our previous reports,^{35,37} on zinc(II)-salen complexes, effect of different substituents at the aromatic spacer (X= H, CH₃, Cl etc.) were studied and the complexes were shown to exhibit hexagonal, rectangular and oblique columnar mesophases of different symmetries. While complexes without any substituent or with an electron donating methyl group at the aromatic spacer exhibited monotropic phase behaviour, electron withdrawing substituent (Cl) at the spacer stabilized the mesophase and enantiotropic phase behaviour was observed. Enhanced dipolar interactions due to electron withdrawing group has been argued in favour of a better core-core correlations with an increase in the clearing temperature than analogous compounds with methyl or without any substituent.

The XRD spectrum recorded at 30°C (Figure 3b) was quite similar to that recorded at high temperatures. However, the diffractogram consisted of additional reflections which agree with the assignment of the Col₁ phase; the presence of diffuse reflections at wide angles and the absence of any mixed-index reflections at low angles rules out the phase to be crystalline in nature at this temperature. Further, the core-core peak becomes much stronger. Inserting the full width at half-maximum value of this reflection, in the standard Scherer equation yields a correlation length of about 115 Å, associated with the stacking of about 28 molecules along the columns. It may also be mentioned that the calculated inter-layer distance in the mesophase; $d = 34.1\text{Å}$, is greater than the DFT computed radius ($\sim 23.9\text{Å}$) of the fully extended half-disc shaped molecule. Though additional information regarding the stacking of the molecular cores in the mesophase is not available, it is presumed that the half-disc shaped molecules

might perhaps preferably arrange themselves in an anti-parallel partially interdigitated manner within the layer (Figure 4).^{56, 57}

2.3 Photophysical properties

The UV-visible absorption and photoluminescence spectra of the compounds recorded in chloroform, CHCl₃ (2×10^{-5} M) at room temperature have been shown in Figure 5 a and b and the data are summarized in Table 3. The UV-visible absorption spectra of the ligands (ndap; n = 12, 14, 16) consisted of two intense absorption bands centered at ~ 278 and ~ 310 nm, attributed to π - π^* transition localized on the aromatic rings (Figure 5a). Another less intense band at ~ 386 nm may be attributed to n- π^* excitation of the C=N fragment. Upon complexation, former two bands were red-shifted to ~ 287 and ~ 329 nm, respectively, with appearance of an additional shoulder at ~ 346 nm, while the low intensity band due to n- π^* transition in the ligand disappeared because of the participation of the nitrogen's lone pair in coordination to the Zn²⁺ ion. The photoluminescent spectra of the ligands and Zn(II)-salen complexes were recorded at room temperature in CHCl₃ solution (2×10^{-5} M), mesophase and also in the solid state (Figure 5b). The ligands are non-emissive. The solid state emission spectra of the complexes were recorded by placing a uniform powder sheet between two quartz plates. The complexes showed blue luminescence with emission maxima centered at ~ 424 nm and emission quantum yield of $\sim 23\%$ (solution), and $\sim 5\%$ (solid) under UV irradiation (330 nm). The observed fluorescence emission originates from metal-perturbed π - π^* ligand-centered transitions. With respect to solution, the position of the emission maxima is virtually unaltered in the solid state. However, the emission intensity quenches substantially following closer association of molecular cores in the solid state as compared to the solution. In POM study, the mesophase of the Zn(II) complex that developed at 125 °C during the cooling cycle freezes into a glassy state persisting till ambient temperature enabling photoluminescence study in the mesophase ($\lambda_{\text{max}} \approx 425$ nm) as well. Similar studies in the frozen glassy state were made earlier for

related complexes.³⁴ The emission energies are virtually un-affected in the solid, solution and in the mesophase (Figure 5b).

Notably, the nature of substituent also have marked influence on the emission behavior of such complexes. When compared to systems with methyl or un-substituted aromatic spacer group, a distinct red shift (~ 40 nm) of the emission band has been noticed in going from the un-substituted zinc(II) complex to the chloro-substituted one.³⁵⁻³⁷ This is believed to be arising from the electron withdrawing effect of the chloro group on the π - π^* transition of the corresponding complex. The observed photophysical behaviour is consistent with those reported for Zn(II) complexes of Schiff bases substituted with electron donating/withdrawing groups.⁵⁸ Emission maxima of complexes with differently substituted (X = H, CH₃, Cl) aromatic spacers studied earlier³⁵⁻³⁷ were observed at > 500 nm. In the present case of methyl substituted aliphatic bridges, the emissions were significantly blue shifted to ~ 424 nm consistent with the enhanced flexibility.

UV-visible and photoluminescent spectra of the Zn(II)-salen complexes (Figure 6 a and b) were also recorded in dilute solutions (2×10^{-5} M) of different coordinating and non-coordinating solvents in order to study the de-aggregation/ aggregation phenomena. The absorption spectra recorded in non-coordinating solvents (e.g. CH₂Cl₂, CHCl₃ and toluene) consisted of two well-defined bands located at ~ 287 nm, 331nm and a shoulder at 345nm (Figure 6a) attesting formation of aggregates.^{53,54} In coordinating solvent (THF), a red shift (~ 14 nm) of the longer wavelength feature is observed due to the axial coordination of the solvent molecules, suggesting de-aggregation (Figure 6a).^{53,54} The coordinatively unsaturated Zn²⁺ ion behaves as a Lewis acid. This behavior is unlike to that observed in case of symmetrical molecule containing ethylene diamine spacer wherein upon de-aggregation; a blue shift of longer absorption feature was noticed.⁵² A rather unusual optical behavior is attributed to the lack of conjugation between the J-type aggregated salen moieties. Methyl group being electron donating in nature induces a considerable amount of conjugation (+I effect) in the ligand framework in the present complexes. Also the tetrahedral methyl

group due to its steric requirement tends to restrict salicylidene groups of each unit in the dimer to H-type aggregate (Figure 6c). Similar results were obtained in other related systems with conjugated aliphatic and aromatic spacers.^{53,54} Concentration variations had virtually no effect on these features up to a concentration of 1×10^{-4} M (Figure 7). Photoluminescent spectra of the complexes (Figure 6b) recorded in non-coordinating solvents exhibited a broad band at ~ 424 nm. In coordinating solvents, the maxima is slightly red shifted (~ 8 nm) with enhancement in fluorescent intensity suggesting de-aggregation with concomitant formation of 1:1 adduct.^{53,54} The emission quantum yield values in non-coordinating solvents (e.g. CH_2Cl_2 , CHCl_3 and toluene) are around 22% which were enhanced (EQY = 38%) upon de-aggregation in coordinating solvent. Fluorescence of face-to-face-stacked H-type dimer aggregates (sandwich-type dimers) are known to be quenched relative to that of the monomer.⁵⁹ A rapid energy relaxation of the lower excited states causes this fluorescence suppression. The absorption or emission characteristics of the complexes are invariant of the alkyl chain lengths (Table 3).

In order to minimize inter-electronic repulsions, Zn(II) ion prefers a tetrahedral geometry to a square planar coordination. However, a short rigid central spacer with steric demands in the present complexes forces the metal center to acquire unfavourable distorted planar geometry which eventually lead to a dimer, $[\text{ZnL}]_2$ ⁶⁰ instead of more stable helical shape formed by tetrahedral 2:2 metal-to-ligand complex, $[\text{Zn}_2\text{L}_2]$.⁶¹

2.4. DFT study

In absence of diffraction quality single crystals, density functional theory (DFT) calculations were carried out on a representative Zn(II) complex (Zn-16dap) employing GAUSSIAN 09 program package⁶² to arrive at the optimized electronic structure. The ground state geometry optimization in the gas phase of the zinc complex has been performed using the three-parameter fit of Becke's hybrid functional combined with the Lee-Yang-Parr correlation functional termed as B3LYP hybrid,^{63,64} generalized gradient approximation (GGA) exchange along with 6-311+G(d,p), 6-31+G(d,p), 6-31G(d) and 6-31G basis sets⁶⁵

for Zn, N and O, C and H, respectively, without imposing any symmetry constrain. Appropriate structure of the complex was confirmed as energy minima by calculating the vibrational frequency and confirming the absence of any imaginary frequencies. Based on the optimized geometry of the zinc complex, TD-DFT calculations on an isolated molecule of the title complex (Zn-16dap) have been performed at the B3LYP level to study the spectroscopic and electronic properties. Since the electronic absorption spectra of the compounds were recorded in dichloromethane, the solvent effects were taken into consideration in the theoretical modelling. GAUSSSUM⁶⁶ program was employed to calculate the individual contribution of various groups to each molecular orbital. A solvation method of the polarisable continuum model (PCM)⁶⁷ using the integral equation formalism (IEF) variant⁶⁸ were considered in calculations. Important geometric parameters of the optimized Zn(II) complex as evaluated by DFT at B3LYP level are collected in Table 4. Average Zn—O and Zn—N bond lengths of the Zn(II) complex are calculated to be 1.931 and 2.077Å, respectively. The O1—Zn—O2 and N1—Zn—N2 bond angles are found to be 108.9° and 80.0° respectively. The O1—Zn—N1, O2—Zn—N2, O1—Zn—N2 and O2—Zn—N1 bond angles are calculated to be 91.9°, 92.1°, 148.6° and 148.8°, respectively, around the zinc atom indicating a distorted square planar geometry (Figure 8). The dihedral angle O1—N3—N2—O2 as evaluated from DFT calculation is about 39.7° reflecting a deviation from planarity.

The three-dimensional (3D) iso-surface plots of the lowest unoccupied molecular orbitals (LUMOs) and the highest occupied molecular orbitals (HOMOs) of the zinc complex are presented in Figure 9. The electron density of the HOMO is localized almost entirely on the aromatic rings, while that of the LUMO is mainly centered on both N=C bonds and aromatic rings. The HOMO and LUMO energies are calculated to be -5.58 eV and -1.41 eV, respectively, the energy difference being $\Delta E = 4.17$ eV. This value is somewhat higher than the HOMO–LUMO energy difference value ($\Delta E = 3.60$ eV) evaluated from the lowest energy UV-Vis band (346nm). Extensive intermolecular interactions in the solution phase (UV-Vis study) as against a free gaseous molecule (DFT study) could be one plausible reason for such a deviation. While ligand p_{π} orbitals contribute almost entirely to HOMO-1(98%), HOMO-2(99%),

HOMO-3(100%) orbitals, HOMO-4 orbital receives a negligible contribution from metal d_{π} orbitals(8%). Electron density on LUMO+1, LUMO+3 and LUMO+4 orbitals is mainly due to ligand p_{π}^* orbitals while that on LUMO+2 is primarily due to metal d_{π}^* orbitals(87%).

TD-DFT calculations have been carried out for the Zn-16dap complex to account for the observed bands in the UV-visible region. The key electronic transitions, corresponding oscillator strength (f), orbitals involved in these transitions and their percentage contribution to each transition are summarized in Table 5. The surface of each peak in the spectra is proportional to oscillator strength (f), which also reveals the probability of electronic transition. The title complex exhibits three absorption bands at 345, 336 and 295nm, respectively. The absorption band at 345nm corresponds to HOMO→LUMO electronic transition owing to the $L(\pi) \rightarrow L(\pi^*)$, where HOMO corresponds to π bonding orbitals of aromatic rings of the ligand and LUMO corresponds to π^* (anti-bonding) orbitals of the aromatic rings (intra-ligand charge transfer). This transition is consistent with the experimental value of 346nm. The high energy absorption bands of the complex occur at 336 and 295nm, which could be assigned to HOMO-1→LUMO and HOMO-2→LUMO electronic transitions, predominantly due to intra-ligand ($\pi \rightarrow \pi^*$) charge transfer. These two transitions resemble the experimental value of 331 and 286nm, respectively.

3. Conclusion

A series of new Zn(II) complexes of ‘salen’ type asymmetric Schiff base ligands bearing long pendant alkoxy arm at the 4-position of side aromatic rings and an asymmetric central spacer group have been accessed. Co-ordination of Zn^{2+} ion to the ligands induces lamello-columnar mesomorphism in otherwise non-mesomorphic ligands. These half-disc shaped molecules assemble in an anti-parallel interdigitated manner within the layer in the mesophase. Metal coordination also brings about interesting fluorescent properties in solid state, solution and as well as in the mesophase. In addition, the complexes also exhibit

aggregation behaviour in dilute solutions of different non-coordinating and coordinating solvents suggesting the Lewis acidity of the metal ion in the newly synthesized complexes. Asymmetric methyl substitution at the aliphatic spacer leads to variation in photophysical behaviour and mesophase order in the present complexes as compared to symmetric molecules containing ethylenediamine spacer. The coordinative unsaturation of Zn(II)-complexes may be utilized for binding with other suitable donor groups to tune the properties.

4. Experimental Section

4.1. Physical measurements

The C, H and N analyses were carried out using Elementar Vario EL III Carlo Erba 1108 elemental analyser. The $^1\text{H-NMR}$ spectra were recorded on a Bruker Avance II, 400 MHz spectrometer in CDCl_3 (chemical shift in δ) solution with TMS as internal standard. Ultraviolet-visible absorption spectra of the compounds were recorded on a JASCO V-670 Spectrophotometer. Photoluminescence spectra were recorded on a Perkin Elmer LS 45 Fluorescence Spectrometer. The fluorescence emission quantum yield (EQY) in degassed dichloromethane solutions were determined by the standard optically dilute method⁶⁹ using 9,10-diphenylanthracene (EQY= 0.96, in cyclohexane) as standard.⁷⁰ Quantum yield in the solid state was measured by means of an integrating sphere, in which the solid sample film was prepared via spin coating and was excited by a 20 kW pulsed Xenon source coupled with Monk-Gillieson type monochromators for selecting wavelengths. The resulting luminescence was acquired by an intensified charge-coupled detector for subsequent analyses. Infrared spectra were recorded on a Perkin Elmer BX series spectrometer on KBr disc in the $400\text{--}4000\text{ cm}^{-1}$ range. The optical textures of the different phase of the compounds were studied using a Nikon ECLIPSE LV100 POL polarizing microscope attached with Instec hot and cold stage HCS402, with STC200 temperature controller of 0.1°C accuracy. The thermal behaviour of the compounds were studied using a Pyris-1 system linked to a Perkin Elmer differential scanning calorimeter (DSC) with a heating or cooling rate of $5^\circ\text{C}/\text{min}$. X-ray diffraction (XRD) studies

were carried out using samples filled in Lindemann capillaries. The apparatus essentially involved a high-resolution X-ray powder diffractometer (PANalytical X'Pert PRO) equipped with a high-resolution fast detector PIXCEL. Quantum chemical calculation on Zn(II) complex was performed using density functional theory (DFT) as implemented in GAUSSIAN 09 package.

4.2. Materials

The materials were procured from Tokyo Kasei, Japan and Lancaster Chemicals, USA. All solvents were purified and dried using standard procedures. Silica (60-120 mesh) from Spectrochem was used for chromatographic separation. Silica gel G (E-Merck, India) was used for TLC.

4.3. Synthesis and analysis

4.3.1. Synthesis of *n*-alkoxysalicylaldehyde (*n* = 12, 14, 16).

2,4-Dihydroxybenzaldehyde (10 mmol, 1.38g), KHCO_3 (10 mmol, 1g), KI (catalytic amount) and 1-bromododecane (10 mmol, 2.4g) or 1-bromotetradecane (10 mmol, 2.5g) or 1-bromohexadecane (10 mmol, 2.8g) were mixed in 250 mL of dry acetone and the mixture was heated under reflux for 24 h, and then filtered, while hot, to remove any insoluble solids. Dilute HCl was added to neutralize the warm solution and then extracted with chloroform (100mL). The combined chloroform extract was concentrated to give a purple solid. The solid was purified by column chromatography using a mixture of chloroform and hexane (v/v, 1/1) as eluent. Evaporation of the solvents afforded a white solid product.

4.3.2. Synthesis of *N,N'*-bis(4-(4'-*n*-alkoxy)-salicylidene)-1,2-diaminopropane (*ndap*), *n* = 12, 14 or 16

General procedure:

Schiff bases (*ndap*) were prepared by adding ethanolic solution of 2-hydroxy-4-(*n*-alkoxy)salicylaldehyde (1 mmol) to ethanolic solution of 1,2-diaminopropane (0.5 mmol). The solution mixture was heated under reflux with a few drops of acetic acid as catalyst for 3h to yield the light yellow Schiff base, *N,N'*-bis(4-

(4'-n-alkoxy)-salicylidene)-1,2-diaminopropane. The product was collected by filtration and recrystallized from absolute ethanol to obtain a pure compound.

4.3.3. *N, N'*-bis(4-(4'-n-dodecyloxy)-salicylidene)-1,2-diaminopropane (12dap).

Yield = 0.23g (74%); Anal. Calc. for $C_{41}H_{66}N_2O_4$ (651): C, 75.65; H, 10.22; N, 4.30. Found: C, 75.63; H, 10.21; N, 4.33. %. 1H NMR (400 MHz, $CDCl_3$; Me_4Si at $25^\circ C$, ppm): δ = 11.45 (s, 1H, H^7), 8.21 (s, 1H, H^1), 8.17 (s, 1H, $H^{1'}$), 7.01-6.72 (m, 4H, H^2 , H^3), 6.21 (s, 2H, H^4), 3.98 (t, $^3J_{H,H} = 8Hz$, 4H, O- CH_2), 3.70-3.63 (m, 2H, H^5), 1.68 (m, 3H, H^6), 1.35-1.30 (m, 1H, H^7), 1.22-1.03 (m, - CH_2 of methylene proton in side chain), 0.89 (t, $^3J_{H,H} = 8Hz$, 6H, - CH_3). IR (ν_{max} , cm^{-1} , KBr): 3370 (ν_{OH}), 2923 ($\nu_{as(C-H)}$, CH_3), 2857 ($\nu_{s(C-H)}$, CH_3), 1653 ($\nu_{C=N}$), 1227 (ν_{C-O}).

4.3.4. *N, N'*-bis(4-(4'-n-tetradecyloxy)-salicylidene)-1,2-diaminopropane (14dap).

Yield = 0.29g (77%); Anal. Calc. for $C_{45}H_{74}N_2O_4$ (707.1): C, 76.44; H, 10.55; N, 3.96. Found: C, 76.47; H, 10.57; N, 3.95. %. 1H NMR (400 MHz, $CDCl_3$; Me_4Si at $25^\circ C$, ppm): δ = 11.43 (s, 1H, H^7), 8.23 (s, 1H, H^1), 8.20 (s, 1H, $H^{1'}$), 7.03-6.75 (m, 4H, H^2 , H^3), 6.23 (s, 2H, H^4), 3.98 (t, $^3J_{H,H} = 8Hz$, 4H, O- CH_2), 3.72-3.65 (m, 2H, H^5), 1.67 (m, 3H, H^6), 1.34-1.27 (m, 1H, H^7), 1.22-1.01 (m, - CH_2 of methylene proton in side chain), 0.89 (t, $^3J_{H,H} = 8Hz$, 6H, - CH_3). IR (ν_{max} , cm^{-1} , KBr): 3372 (ν_{OH}), 2922 ($\nu_{as(C-H)}$, CH_3), 2854 ($\nu_{s(C-H)}$, CH_3), 1655 ($\nu_{C=N}$), 1225 (ν_{C-O}).

4.3.5. *N, N'*-bis(4-(4'-n-hexadecyloxy)-salicylidene)-1,2-diaminopropane (16dap).

Yield = 0.31g (77%); Anal. Calc. for $C_{49}H_{82}N_2O_4$ (763.2): C, 77.11; H, 10.83; N, 3.67. Found: C, 77.13; H, 10.81; N, 3.70. %. 1H NMR (400 MHz, $CDCl_3$; Me_4Si at $25^\circ C$, ppm): δ = 11.47 (s, 1H, H^7), 8.22 (s, 1H, H^1), 8.19 (s, 1H, $H^{1'}$), 7.01-6.74 (m, 4H, H^2 , H^3), 6.25 (s, 2H, H^4), 3.98 (t, $^3J_{H,H} = 8Hz$, 4H, O- CH_2), 3.77-3.58 (m, 2H, H^5), 1.66 (m, 3H, H^6), 1.35-1.28 (m, 1H, H^7), 1.27-1.00 (m, - CH_2 of methylene proton

in side chain), 0.88 (t, $^3J_{H,H} = 8\text{Hz}$, 6H, $-\text{CH}_3$). IR (ν_{max} , cm^{-1} , KBr): 3371(ν_{OH}), 2924 ($\nu_{\text{as(C-H)}}$, CH_3), 2856 ($\nu_{\text{s(C-H)}}$, CH_3), 1654 ($\nu_{\text{C=N}}$), 1225 ($\nu_{\text{C-O}}$).

4.3.6. Synthesis of Zinc (II) complexes (Zn-ndap, n=12, 14, 16)

General procedure:

The ligand 12dap (0.06g, 0.1mmol) or 14dap (0.07g, 0.1mmol) or 16dap (0.08g, 0.1mmol) was dissolved in minimum volume of absolute ethanol. To this, an equimolar amount of zinc acetate $\text{Zn}(\text{OAc})_2 \cdot 2\text{H}_2\text{O}$ (0.02g, 0.1mmol) in methanol was then added slowly and stirred for 3h at room temperature. A white solid formed in each case, was filtered, washed with diethyl ether and re-crystallized from chloroform-ethanol (1:1).

4.3.7. Zn-12dap:

Yield = 0.05g (75%); Anal. Calc. for $\text{C}_{41}\text{H}_{64}\text{N}_2\text{O}_4\text{Zn}$ (714.3): C, 68.94; H, 9.03; N, 3.92. Found: C, 68.91; H, 9.07; N, 3.95. %. ^1H NMR (400 MHz, CDCl_3 ; Me_4Si at 25°C , ppm): $\delta = 7.65$ (s, 1H, H^1), 7.63 (s, 1H, $\text{H}^{1'}$), 6.97-6.70 (m, 4H, H^2 , H^3), 6.26 (s, 2H, H^4), 3.99 (t, $^3J_{H,H} = 8\text{Hz}$, 4H, O-CH_2), 3.73-3.67 (m, 2H, H^5), 1.65 (m, 3H, H^6), 1.36-1.31 (m, 1H, H^7), 1.26-0.99 (m, $-\text{CH}_2$ of methylene proton in side chain), 0.88 (t, $^3J_{H,H} = 8\text{Hz}$, 6H, $-\text{CH}_3$). IR (ν_{max} , cm^{-1} , KBr): 2919 ($\nu_{\text{as(C-H)}}$, CH_3), 2853 ($\nu_{\text{s(C-H)}}$, CH_3), 1639 ($\nu_{\text{C=N}}$), 1215 ($\nu_{\text{C-O}}$).

4.3.8. Zn-14dap:

Yield = 0.06g (78%); Anal. Calc. for $\text{C}_{45}\text{H}_{72}\text{N}_2\text{O}_4\text{Zn}$ (770.5): C, 70.15; H, 9.42; N, 3.64. Found: C, 70.14; H, 9.45; N, 3.65. %. ^1H NMR (400 MHz, CDCl_3 ; Me_4Si at 25°C , ppm): $\delta = 7.68$ (s, 1H, H^1), 7.66 (s, 1H, $\text{H}^{1'}$), 6.99-6.71 (m, 4H, H^2 , H^3), 6.27 (s, 2H, H^4), 3.99 (t, $^3J_{H,H} = 8\text{Hz}$, 4H, O-CH_2), 3.76-3.60 (m, 2H, H^5), 1.70 (m, 3H, H^6), 1.37-1.26 (m, 1H, H^7), 1.27-1.07 (m, $-\text{CH}_2$ of methylene proton in side chain), 0.89 (t, $^3J_{H,H} = 8\text{Hz}$, 6H, $-\text{CH}_3$). IR (ν_{max} , cm^{-1} , KBr): 2921 ($\nu_{\text{as(C-H)}}$, CH_3), 2856 ($\nu_{\text{s(C-H)}}$, CH_3), 1639 ($\nu_{\text{C=N}}$), 1217($\nu_{\text{C-O}}$).

4.3.9. Zn-16dap:

Yield = 0.06g (77%); Anal. Calc. for $C_{49}H_{80}N_2O_4Zn$ (826.6): C, 71.20; H, 9.76; N, 3.39. Found: C, 71.17; H, 9.78; N, 3.40 %. 1H NMR (400 MHz, $CDCl_3$; Me_4Si at $25^\circ C$, ppm): δ = 7.67 (s, 1H, H^1), 7.64 (s, 1H, $H^{1'}$), 7.00-6.73 (m, 4H, H^2 , H^3), 6.22 (s, 2H, H^4), 3.99 (t, $^3J_{H,H} = 8Hz$, 4H, O- CH_2), 3.74-3.60 (m, 2H, H^5), 1.64 (m, 3H, H^6), 1.34-1.24 (m, 1H, H^7), 1.28-0.98 (m, - CH_2 of methylene proton in side chain), 0.87 (t, $^3J_{H,H} = 8Hz$, 6H, - CH_3). IR (ν_{max} , cm^{-1} , KBr): 2917 ($\nu_{as(C-H)}$, CH_3), 2854 ($\nu_{s(C-H)}$, CH_3), 1637 ($\nu_{C=N}$), 1215 (ν_{C-O}).

Acknowledgments

SC and PM acknowledges Department of Science and Technology (DST), New Delhi, Government of India for the INSPIRE Junior Research Fellowship (Code: IF110692) and financial support (SR/FT/CS-86/2010), respectively. Sophisticated Analytical Instrumentation Facility (SAIF), North Eastern Hill University, Shillong and Central Drug Research Institute (CDRI), Lucknow are acknowledged for some spectral results. Authors are also thankful to DBT e-Library Consortium (DeLCON) of Bio-Informatics Centre, Assam University, India.

References

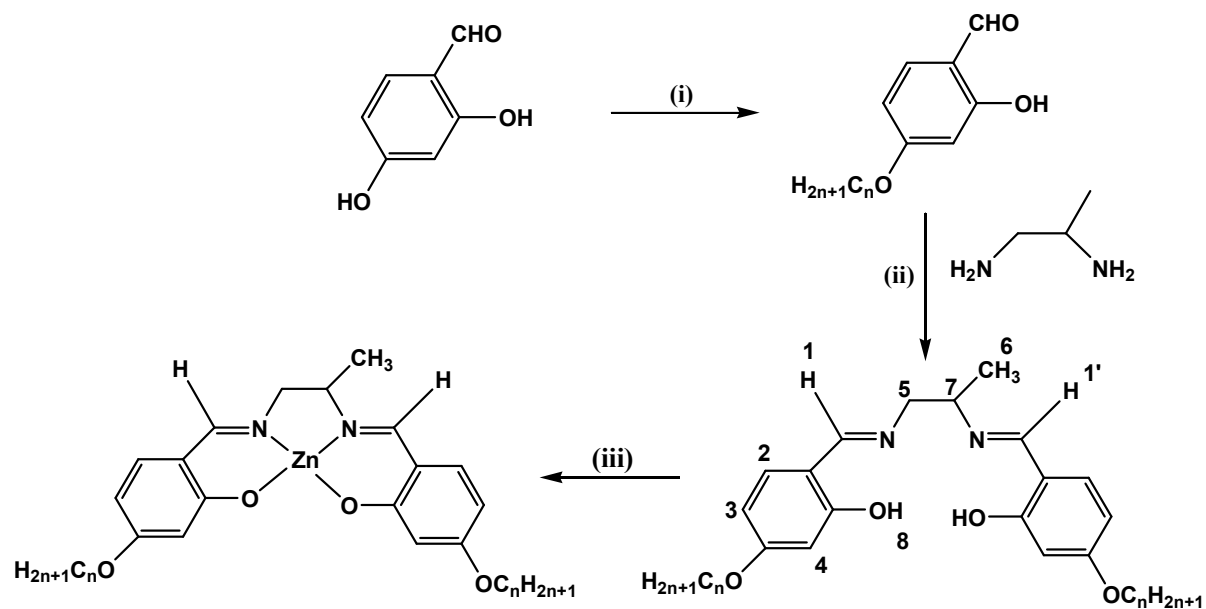
1. A.W. Kleij, *Eur. J. Inorg. Chem.*, 2009, 193–205.
2. A.W. Kleij, *Chem. Eur. J.*, 2008, **14**, 10520–10529.
3. S.J. Wezenberg and A.W. Kleij, *Angew. Chem. Int. Ed.*, 2008, **47**, 2354–2364.
4. G.H. Clever and T. Carell, *Angew. Chem. Int. Ed.*, 2007, **46**, 250–253.
5. K.C. Gupta and A.K. Sutar, *Coord. Chem. Rev.*, 2008, **252**, 1420–1450.
6. P.G. Cozzi, *Chem. Soc. Rev.*, 2004, **33**, 410–421.
7. L. Canali and D.C. Sherrington, *Chem. Soc. Rev.*, 1999, **28**, 85–93.
8. E.N. Jacobsen, in *Catalytic Asymmetric Synthesis*, ed. I. Ojima, VCH, New York, 1993, pp. 159.
9. G. Barone, N. Gambino, A. Ruggirello, A. Silvestri, A. Terenzi and V.T. Liveri, *J. Inorg. Biochem.*, 2009, **103**, 731–737.
10. Y. Kou, J. Tian, D. Li, W. Gu, X. Liu, S. Yan, D. Liao and P. Cheng, *Dalton Trans.*, 2009, 2374–2382.
11. A. Silvestri, G. Barone, G. Ruisi, D. Anselmo, S. Riela and V.T. Liveri, *J. Inorg. Biochem.*, 2007, **101**, 841–848.
12. C. Liu, M. Wang, T. Zhang and H. Sun, *Coord. Chem. Rev.*, 2004, **248**, 147–168.
13. J. Cheng, K. Wei, X. Ma, X. Zhou and H. Xiang, *J. Phys. Chem. C.*, 2013, **117**, 16552–16563.
14. V. Liuzzo, W. Oberhauser and A. Pucci, *Inorg. Chem. Commun.*, 2010, **13**, 686–688.
15. H.-C. Lin, C.-C. Huang, C.-H. Shi, Y.-H. Liao, C.-C. Chen, Y.-C. Lin and Y.-H. Liu, *Dalton Trans.*, 2007, 781–791.
16. E. Hadjoudis and I.M. Mavridis, *Chem. Soc. Rev.*, 2004, **33**, 579–588.
17. M. Andruh, *Chem. Commun.*, 2011, **47**, 3025–3042.
18. H. Miyasaka, A. Saitoh and S. Abe, *Coord. Chem. Rev.*, 2007, **251**, 2622–2664.
19. I.P. Oliveri, S. Failla, A. Columbo, C. Dragonetti, S. Righetto and S. Di Bella, *Dalton Trans.*, 2014, **43**, 2168–2175.

20. S. Di Bella, I.P. Oliveri, A. Colombo, C. Dragonetti, S. Righetto and D. Roberto, *Dalton Trans.*, 2012, **41**, 7013–7016.
21. P.G. Lacroix, *Eur. J. Inorg. Chem.*, 2001; 339–348.
22. C. Datta, R. Chakrabarty, G. Das, C.R. Bhattacharjee and P. Mondal, *Liq. Cryst.*, 2013, **41**, 541–551.
23. C.R. Bhattacharjee, C. Datta, G. Das, R. Chakrabarty and P. Mondal, *Polyhedron*, 2012, **33**, 417–424.
24. Y. Abe, Y. Takagi, M. Nakamura, T. Takeuchi, T. Tanase, M. Yokokawa, H. Mukai, T. Megumi, A. Hachisuga and K. Ohta, *Inorg. Chim. Acta*, 2012, **392**, 254–260.
25. A. Ohta, Y. Yamamoto, H. Kamihata, Y.H. Lee, F. Ichikawa, K. Ohta, Y. Abe, N. Hoshino, M. Kojima and S. Hayami, *Inorg. Chem. Commun.*, 2012, **16**, 89–91.
26. C.R. Bhattacharjee, G. Das, P. Mondal, S.K. Prasad and D.S.S. Rao, *Inorg. Chem. Commun.*, 2011, **14**, 606–612.
27. Y. Abe, N. Nakazima, T. Tanase, S. Katano, H. Mukai and K. Ohta, *Mol. Cryst. Liq. Cryst.*, 2007, **466**, 129–147.
28. Y. Abe, K. Nakabayashi, N. Matsukawa, H. Takashima, M. Iida, T. Tanase, M. Sugibayashi, H. Mukai and K. Ohta, *Inorg. Chim. Acta*, 2006, **359**, 3934–3946.
29. K. Binnemans, K. Lodewyckx, T. Cardinaes, T.N. Parac Vogt, C. Bourgogne, D. Guillon and B. Donnio, *Eur. J. Inorg. Chem.*, 2006, 150–157.
30. Y. Abe, H. Akao, Y. Yoshida, H. Takashima, T. Tanase, H. Mukai and K. Ohta, *Inorg. Chim. Acta*, 2006, **359**, 3147–3155.
31. L.L. Li, H.F. Xiang, X.G. Zhou, M.L. Li and D. Wu, *J. Chem. Educ.*, 2012, **89**, 559–560.
32. V.K. Gupta, R.N. Goyal, A.K. Jain and R.A. Sharma, *Electrochim. Acta*, 2009, **54**, 3218–3224.
33. V.K. Gupta, A.K. Jain and G. Maheshwari, *Talanta*, 2007, **72**, 49–53.

34. D. Pucci, I. Aiello, A. Bellusci, A. Crispini, M. Ghedini and M. La Deda, *Eur. J. Inorg. Chem.*, 2009, 4274–4281.
35. C.R. Bhattacharjee, S. Chakraborty, G. Das and P. Mondal, *Liq. Cryst.*, 2012, **39**, 1435–1442.
36. C.R. Bhattacharjee, G. Das, P. Mondal, S.K. Prasad and D.S.S. Rao, *Eur. J. Inorg. Chem.*, 2011, 1418–1424.
37. C.R. Bhattacharjee, G. Das, P. Mondal and N.V.S. Rao, *Polyhedron*, 2010, **29**, 3089–3096.
38. I.P. Oliveri and S. Di Bella, *Tetrahedron*, 2011, **67**, 9446–9449.
39. M.E. Germain and M.J. Knapp, *J. Am. Chem. Soc.*, 2008, **130**, 5422–5423.
40. M.E. Germain, T.R. Vargo, P.G. Khalifah and M.J. Knapp, *Inorg. Chem.*, 2007, **46**, 4422–4429.
41. M. Cano, L. Rodri'guez, J.C. Lima, F. Pina, A.D. Cort, C. Pasquini and L. Schiaffino, *Inorg. Chem.*, 2009, **48**, 6229–6235.
42. A.D. Cort, L. Mandolini, C. Pasquini, K. Rissanen, L. Russo and L. Schiaffino, *New J. Chem.*, 2007, **31**, 1633–1638.
43. S.J. Wezenberg, E.C. Escudero-Ad'an, J. Benet-Buchholz and A.W. Kleij, *Inorg. Chem.*, 2008, **47**, 2925–2927.
44. A.W. Kleij, M. Kuil, D.M. Tooke, A.L. Spek and J.N.H. Reek, *Inorg. Chem.*, 2007, **46**, 5829–5831.
45. M. Kuil, I.M. Puijk, A.W. Kleij, D.M. Tooke, A.L. Spek and J.N.H. Reek, *Chem.–As. J.*, 2009, **4**, 50–57.
46. A.W. Kleij, M. Kuil, D.M. Tooke, M. Lutz, A.L. Spek and J.N.H. Reek, *Chem. Eur. J.*, 2005, **11**, 4743–4750.
47. M. Kuil, P.E. Goudriaan, A.W. Kleij, D.M. Tooke, A.L. Spek and P.W.N.M. van Leeuwen, J.N.H. Reek, *Dalton Trans.*, 2007, 2311–2320.
48. P.G. Cozzi, *Angew. Chem.*, 2003, **115**, 3001–3004.

49. A.A. Vashchenko, L.S. Lepnev, A.G. Vitukhnovskii, O.V. Kotova, S.V. Eliseeva and N.P. Kuz'mina, *Opt. Spectrosc.*, 2010, **108**, 463–465.
50. O.V. Kotova, S.V. Eliseeva, A.S. Averjushkin, L.S. Lepnev, A.A. Vaschenko, A.Y. Rogachev, A.G. Vitukhnovskii and N.P. Kuzmina, *Russ. Chem. Bull. Int. Ed.*, 2008, **57**, 1880–1889.
51. K.H. Chang, C.C. Huang, Y.H. Liu, Y.H. Hu, P.T. Chou and Y.C. Lin, *Dalton Trans.*, 2004, 1731–1738.
52. G. Consiglio, S. Failla, P. Finocchiaro, I.P. Oliveri and S. Di Bella, *Inorg. Chem.*, 2012, **51**, 8409–8418.
53. G. Consiglio, S. Failla, P. Finocchiaro, I.P. Oliveri and S. Di Bella, *Dalton Trans.*, 2012, **41**, 387–395.
54. G. Consiglio, S. Failla, I.P. Oliveri, R. Purrello and S. Di Bella, *Dalton Trans.*, 2009, 10426–10428.
55. A.W. Kleij, *Dalton Trans.*, 2009, 4635–4639.
56. A.G. Serrette, C.K. Lai and T.M. Swager, *Chem. Mater.*, 1994, **6**, 2252–2268.
57. S.T. Trzaska and T.M. Swager, *Chem. Mater.*, 1998, **10**, 438–443.
58. H.-C. Lin, C.-C. Huang, C.-H. Shi, Y.-H. Liao, C.-C. Chen, Y.-C. Lin and Y.-H. Liu, *Dalton Trans.*, 2007, 781–791.
59. M. Kasha, H.R. Rawls and M.A. El-Bayoumi, *Pure Appl. Chem.*, 1965, **11**, 371–392.
60. G. E. Batley and D. P. Graddon, *Aust. J. Chem.*, 1967, **20**, 885–891.
61. S. Mizukami, H. Houjou, Y. Nagawa and M. Kanesato, *Chem. Commun.*, 2003, 1148–1149.
62. M. J. Frisch, G. W. Trucks, H. B. Schlegel, G. E. Scuseria, M. A. Robb, J. R. Cheeseman, G. Scalmani, V. Barone, B. Mennucci, G. A. Petersson, H. Nakatsuji, M. Caricato, X. Li, H. P. Hratchian, A. F. Izmaylov, J. Bloino, G. Zheng, J. L. Sonnenberg, M. Hada, M. Ehara, K. Toyota, R. Fukuda, J. Hasegawa, M. Ishida, T. Nakajima, Y. Honda, O. Kitao, H. Nakai, T. Vreven, J. A. Montgomery, Jr., J. E. Peralta, F. Ogliaro, M. Bearpark, J. J. Heyd, E. Brothers, K. N. Kudin, V.

- N. Staroverov, R. Kobayashi, J. Normand, K. Raghavachari, A. Rendell, J. C. Burant, S. S. Iyengar, J. Tomasi, M. Cossi, N. Rega, J. M. Millam, M. Klene, J. E. Knox, J. B. Cross, V. Bakken, C. Adamo, J. Jaramillo, R. Gomperts, R. E. Stratmann, O. Yazyev, A. J. Austin, R. Cammi, C. Pomelli, J. W. Ochterski, R. L. Martin, K. Morokuma, V. G. Zakrzewski, G. A. Voth, P. Salvador, J. J. Dannenberg, S. Dapprich, A. D. Daniels, Ö. Farkas, J. B. Foresman, J. V. Ortiz, J. Cioslowski and D. J. Fox, *Gaussian 09, Gaussian, Inc.*, Wallingford CT, 2009.
63. A. D. Becke, *J. Chem. Phys.*, 1993, **98**, 5648-5652.
64. C. Lee, W. Yang and R. G. Parr, *Phys. Rev. B*, 1988, **37**, 785-789.
65. P.C. Hariharan and J.A. Pople. *Theor. Chim. Acta*, 1973, **28**, 213–222.
66. N.M. O'Boyle, A.L. Tenderholt and K.M. Langner, *J. Comput. Chem.*, 2008, **29**, 839–845.
67. E. Cance, B. Mennucci and J. Tomasi, *J. Chem. Phys.*, 1997, **107**, 3032–3041.
68. S. Miertus, E. Scrocco and J. Tomasi, *J. Chem. Phys.*, 1981, **55**, 117–129.
69. J. N. Demas, G. A. Crosby, *J. Phys. Chem.*, 1971, **75**, 991–1024.
70. W. R. Ware, W. Rothman, *Chem. Phys. Lett.*, 1976, **39**, 449–453.



Scheme 1. i. $\text{C}_n\text{H}_{2n+1}\text{Br}$, KHCO_3 , KI, dry acetone, Δ , 24h, and ii. glacial AcOH, absolute EtOH, Δ , 3h
iii. $\text{Zn}(\text{OAc})_2 \cdot 2\text{H}_2\text{O}$, MeOH, stir, 3h.

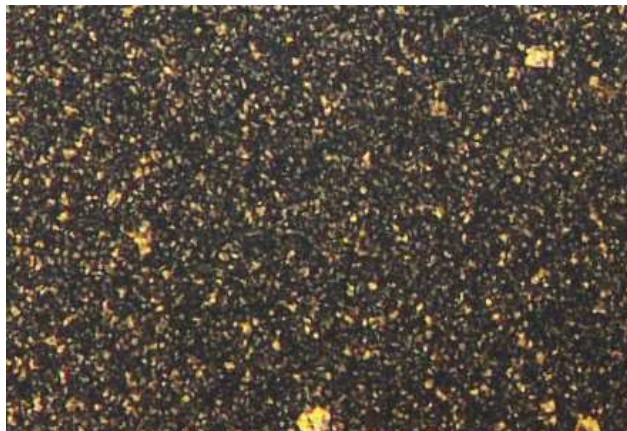


Figure 1. POM image of Zn-16dap upon cooling at 125°C.

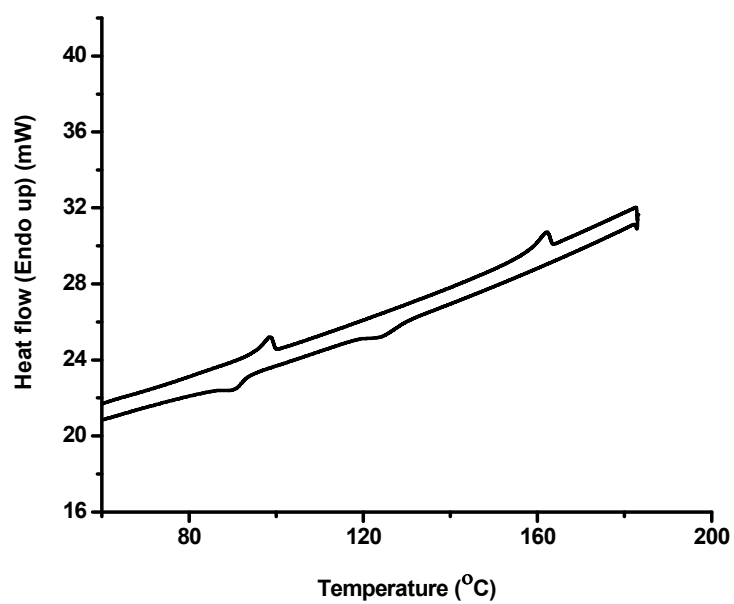
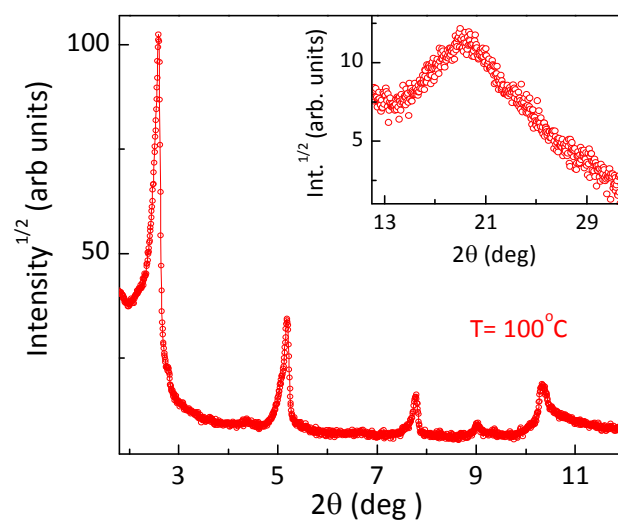
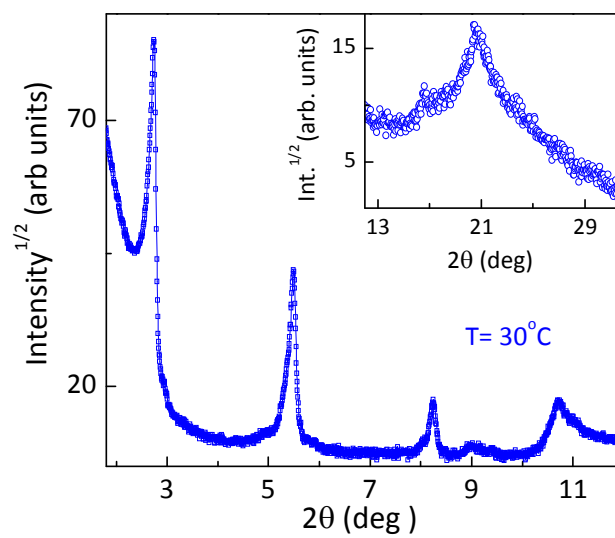


Figure 2. DSC profile of Zn-16dap.



(a)



(b)

Figure 3. PXRD pattern of Zn-16dap at (a) 100 °C and (b) at room temperature (30 °C).

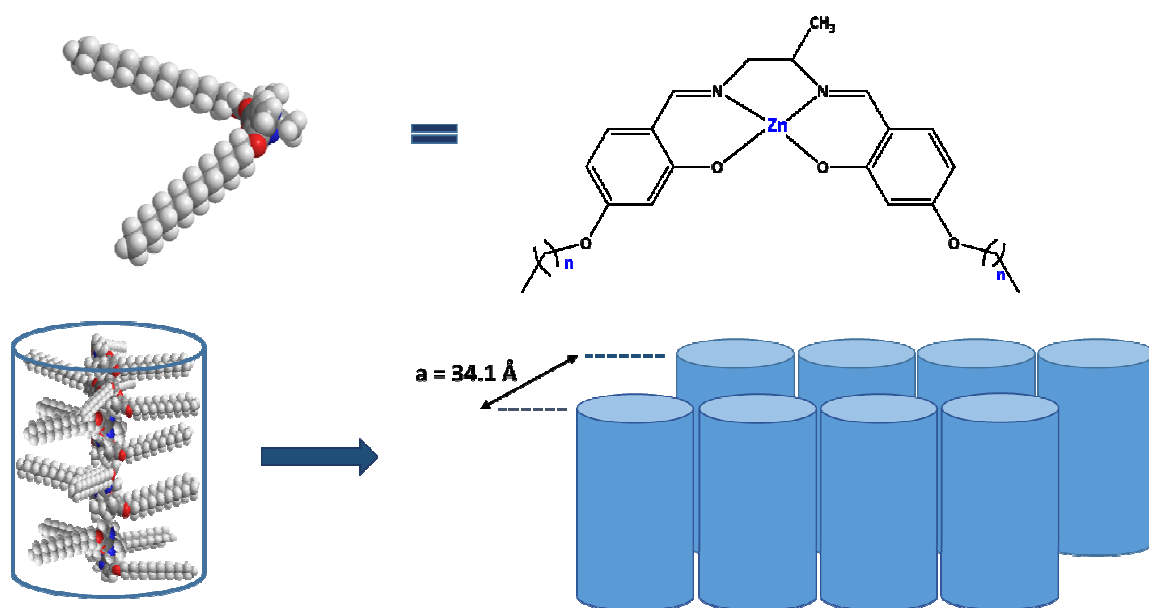


Figure 4. Anti-parallel interdigitated organization of the molecules in lamello-columnar phase.

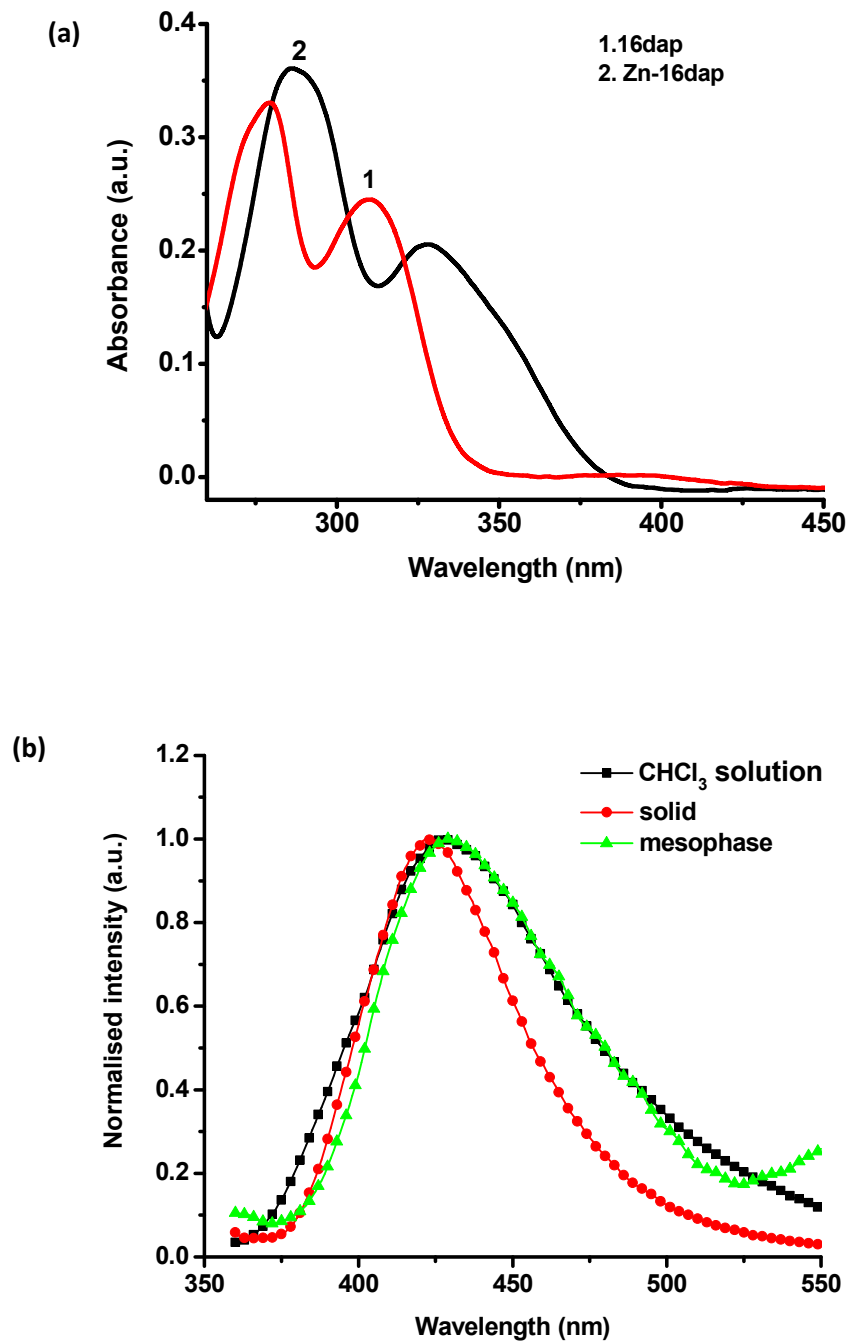
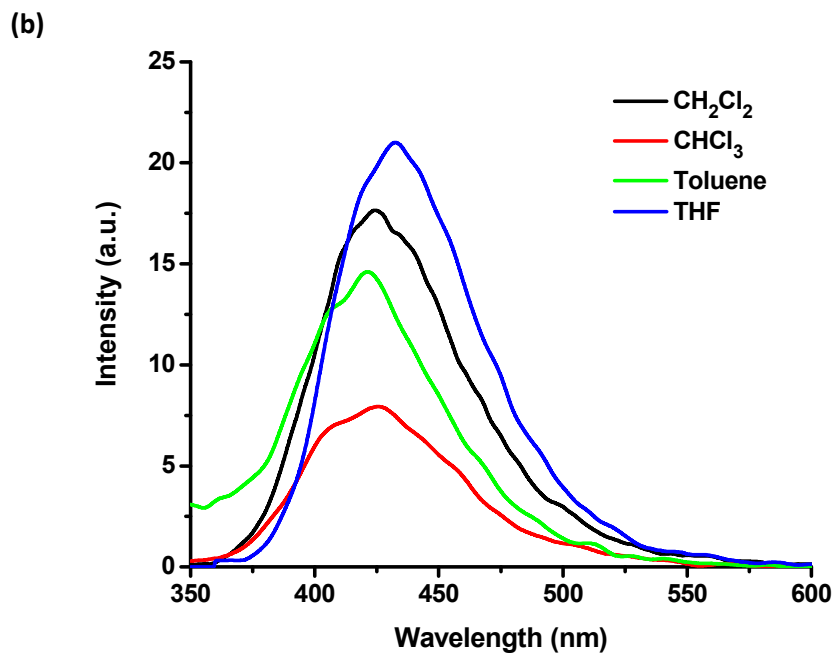
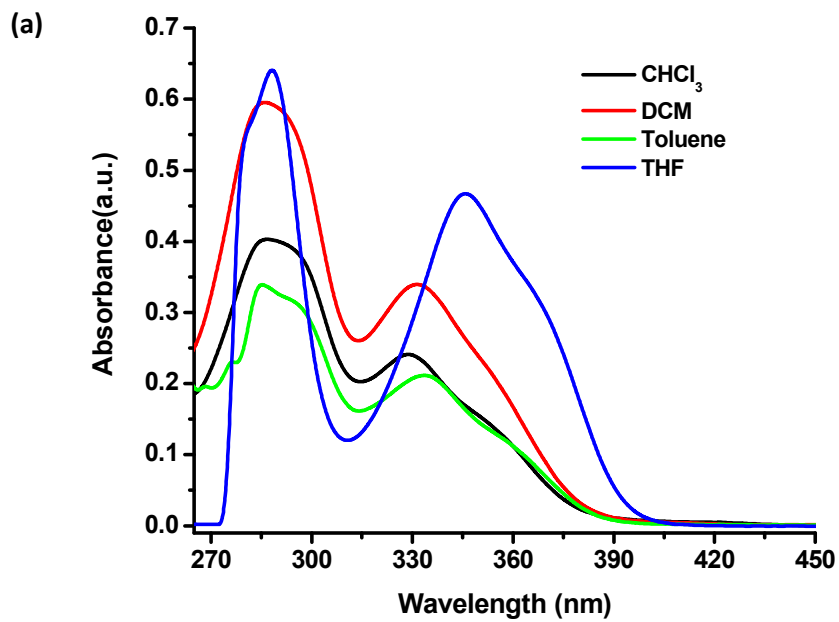


Figure 5. (a) UV-visible absorption spectra of the ligand (16dap) and Zn-16dap in chloroform (2×10^{-5} M) and (b) Intensity (normalized) vs. wavelength photoluminescence profile for the Zn-16dap complex in chloroform solution (2×10^{-5} M), solid state and in mesophase ($\lambda_{\text{ex.}} = 330\text{nm}$).



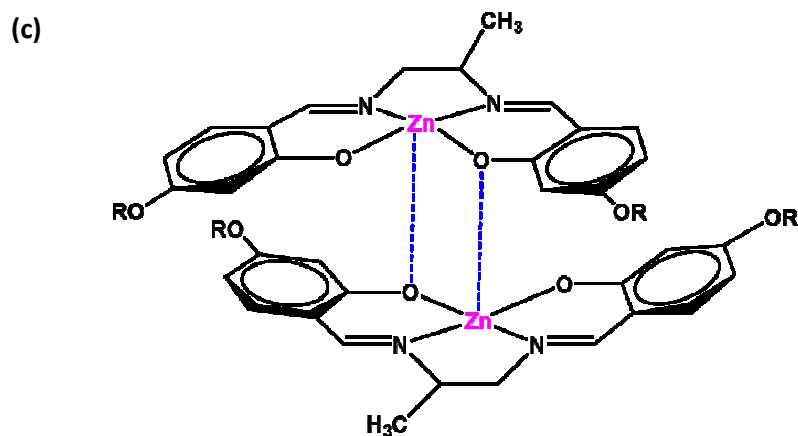


Figure 6. UV-visible absorption spectra (a), fluorescence spectra ($\lambda = 330\text{nm}$; with 10% attenuator) (b) of Zn-16dap ($2 \times 10^{-5}\text{M}$) in different non-coordinating and coordinating solvents and (c) the ‘H-type’ dimer in solution of non-coordinating solvents.

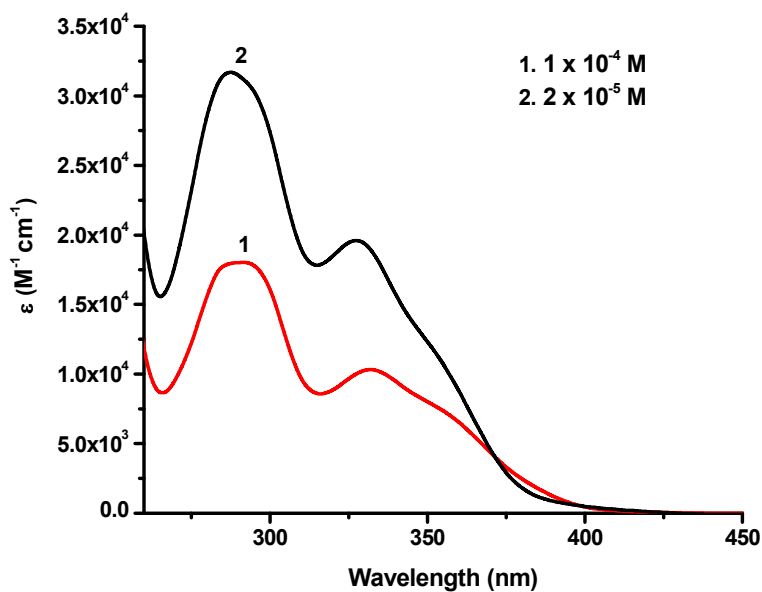


Figure 7. Concentration dependence of UV-visible absorption spectra of Zn-16dap in CHCl_3 solutions.

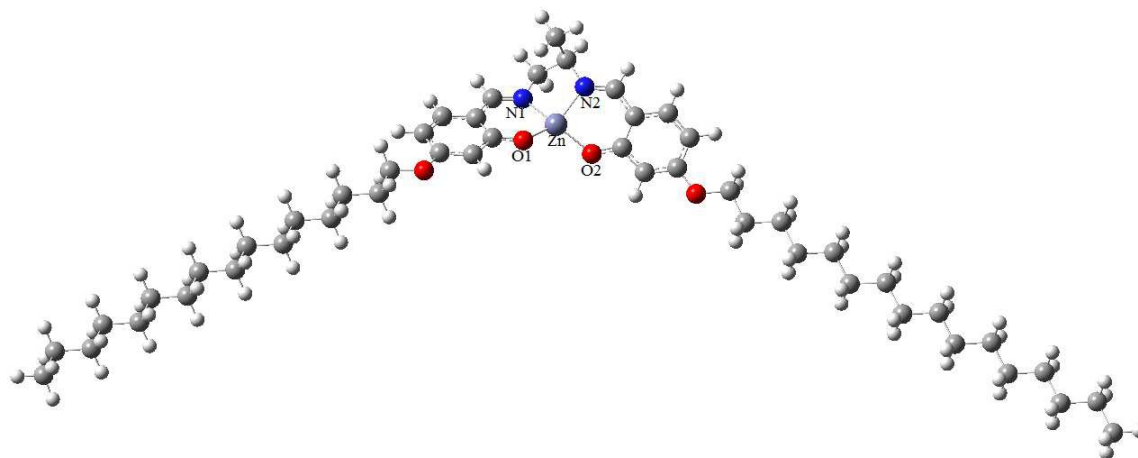


Figure 8. DFT optimized structure of a representative complex, Zn-16dap.

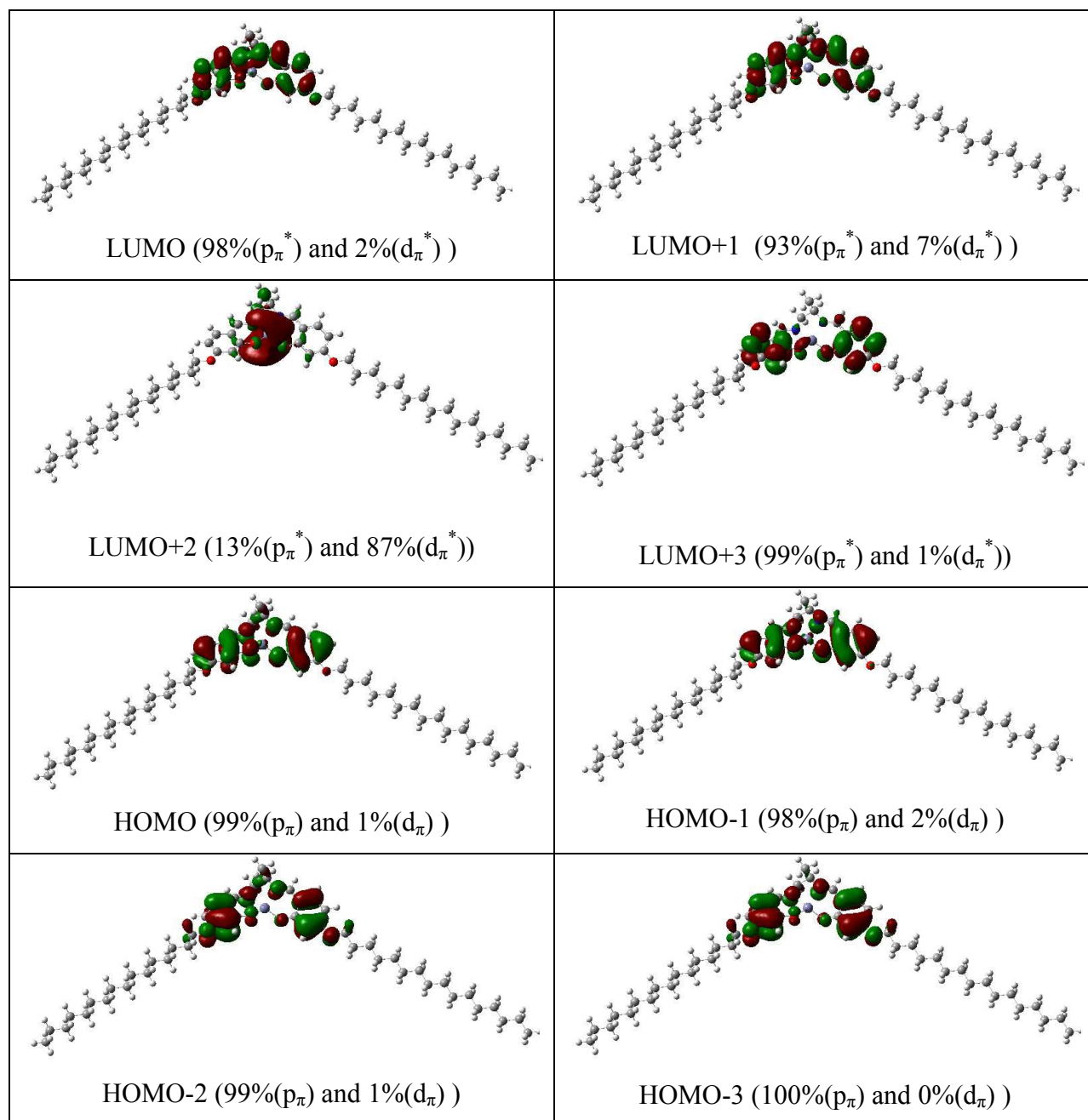


Figure 9. Frontier molecular orbitals of Zn-16dap.

Table 1. Thermodynamic data for the Zn-ndap (n = 12, 14, 16) complexes. Transition temperatures are given in °C, and the corresponding enthalpy changes are in parentheses (ΔH ; kJ mol⁻¹). Cr, Cr₁, Cr₂ refer to phases that are crystalline or solid; Col₁: lamello-columnar phase.

Compounds	Heating ^a	Cooling ^a
Zn-12dap	Cr 94.1(32.8) Cr ₁ 103.4 (2.4) Cr ₂ 134.5 (7.9) Col ₁ 168.6 (1.5) I	I 83.7 (10.1) Cr
Zn-14dap	Cr 97.6 (7.9) Col ₁ 167.4 (14.1) I	I 144.9(12.2) Col ₁ 92.2 (6.3) Cr
Zn-16dap	Cr 98.5 (7.0) Col ₁ 162.1 (8.2) I	I 124.2 (6.2) Col ₁ 90.3 (5.9) Cr

^aDSC peak temperature

Table 2. PXRD data of Zn-16dap.

Temperature (°C)	Parameters	$d_{\text{meas.}}/\text{Å}^{[a, b]}$	$d_{\text{calc.}}/\text{Å}^{[a, b]}$	Miller indices(hkl) ^[c]
At 100 °C	$a = 34.06 \text{ Å}$	34.05 ^s	34.06	100
	$b = 40.46 \text{ Å}$	17.06 ^s	17.03	200
	$V_{\text{cell}} = 5540.5 \text{ Å}^3$	11.37 ^s	11.35	300
	$d = 34.1 \text{ Å}$	9.81 ^s	9.70	140
		8.54 ^s	8.70	240
		4.68 ^d		
		4.02 ^d		
At 30 °C	$a = 32.18 \text{ Å}$	32.19 ^s	32.18	100
	$b = 41.31 \text{ Å}$	16.10 ^s	16.09	200
	$V_{\text{cell}} = 5596.5 \text{ Å}^3$	10.72 ^s	10.73	300
	$d = 32.18 \text{ Å}$	9.87 ^s	9.83	140
		8.24 ^s	8.26	050
		7.87 ^s	7.90	410
		6.51	6.55	350
		5.72	5.76	450
		5.32	5.32	610
		4.29 ^d		
	4.21 ^d			

^[a] $d_{\text{meas.}}$ and $d_{\text{calc.}}$ are the experimentally measured and calculated diffraction spacing, respectively.

^[b] Intensity of the reflections: s; sharp peak, d: diffuse peak. The distances are given in Å. ^[c] $[hkl]$ are the Miller indices of the reflections. For Col₁ phase, $d = (\sum l d_{100})/N_{100}$ where N_{100} is the number of reflections. V_{cell} , is the unit cell volume.

Table 3. UV-visible and photoluminescence spectral data of the ligands (in CHCl₃) and Zn-ndap (n = 12, 14, 16) complexes in different solvents.

Compounds	Solvents	Absorption		Emission
		λ_{max} ; nm	ϵ ; l mol ⁻¹ cm ⁻¹	λ_{max} ; nm
12dap	CHCl ₃	278	16,312	-
		310	12,300	
		386	192	
14dap	CHCl ₃	278	15,936	-
		310	12,305	
		386	200	
16dap	CHCl ₃	279	16,530	-
		310	12,296	
		386	174	
Zn-12dap	CHCl ₃	287	20,359	425
		330	11,240	
		345 ^{sh}	7,875	
	CH ₂ Cl ₂	286	28,967	424
		331	16,543	
		345 ^{sh}	12,756	
	Toluene	287	16,748	421
		333	10,731	
		346 ^{sh}	8,156	
THF	288	31,952	432	
	345	23,675		
	360 ^{sh}	18,789		
Zn-14dap	CHCl ₃	287	19,935	425
		330	10,306	
		347 ^{sh}	7,693	
	CH ₂ Cl ₂	286	28,733	424
		331	16,238	
		347 ^{sh}	13,085	
	Toluene	287	16,892	422
		333	10,736	
		346 ^{sh}	9,712	
THF	288	31,132	433	
	345	22,925		
	361 ^{sh}	19,003		
Zn-16dap	CHCl ₃	287	20,135	425
		329	10,240	
		343 ^{sh}	7,675	
	CH ₂ Cl ₂	286	29,784	424
		331	16,998	
		346 ^{sh}	12,985	
	Toluene	286	16,998	421
		333	10,706	
		345 ^{sh}	8,215	
THF	288	32,082	432	
	345	23,405		
	359 ^{sh}	18,715		

Table 4. Selected bond lengths (Å) and bond angles(°) of Zn-16dap complex optimized at the B3LYP level.

Structural parameter	Bond Lengths (Å) and Bond angles (°)
Zn—O1	1.932
Zn—O2	1.931
Zn—N1	2.076
Zn—N2	2.078
O1—Zn—O2	108.9
N1—Zn—N2	80.0
O1—Zn—N1	91.9
O2—Zn—N2	92.1
O1—Zn—N2	148.6
O2—Zn—N1	148.8
O1—N1—N2—O2	39.7
Molecular length	47.8

Table 5. The experimental absorption bands and the electronic transitions calculated with TD-DFT/B3LYP method of the Zn-16dap complex.

Key transition	Character	λ (nm)	E (eV)	f (Osc. Strength)	Assignments	λ_{exp} (nm) ϵ (l mol ⁻¹ cm ⁻¹)
(90%)HOMO→LUMO	L(π)→L(π^*)	345	3.60	0.124	IL	346 (12,985)
(89%)HOMO-1→LUMO	L(π)→L(π^*)	336	3.70	0.102	IL	331 (16,998)
(85%) HOMO-2→LUMO	L(π)→L(π^*)	295	4.21	0.550	IL	286 (29,784)